Title

The magnitude distribution of dynamically triggered earthquakes

Journal

Geochemistry, Geophysics, Geosystems, 15(9)

Authors

Hernandez, S
Brodsky, EE
Van Der Elst, NJ

Publication Date

2014-09-01

DOI

10.1002/2014GC005404

Peer reviewed

AGU PUBLICATIONS

Geochemistry, Geophysics, Geosystems

RESEARCH ARTICLE
10.1002/2014GC005404

The magnitude distribution of dynamically triggered earthquakes

Stephen Hernandez[1], Emily E. Brodsky[1], and Nicholas J. van der Elst[2]

[1]Department of Earth and Planetary Sciences, University of California, Santa Cruz, Santa Cruz, California, USA, [2]Lamont-Doherty Earth Observatory, Columbia University, Palisades, New York, USA

Key Point:
- Magnitude distributions of triggered and untriggered small quakes are indistinguishable

Supporting Information:
- Readme
- Supplemental_v5_2

Correspondence to:
S. Hernandez,
shernan8@ucsc.edu

Citation:
Hernandez, S., E. E. Brodsky, and N. J. van der Elst (2014), The magnitude distribution of dynamically triggered earthquakes, *Geochem. Geophys. Geosyst.*, *15*, 3688–3697, doi:10.1002/2014GC005404.

Received 5 MAY 2014
Accepted 22 AUG 2014
Accepted article online 27 AUG 2014
Published online 26 SEP 2014

Abstract Large dynamic strains carried by seismic waves are known to trigger seismicity far from their source region. It is unknown, however, whether surface waves trigger only small earthquakes, or whether they can also trigger large earthquakes. To partially address this question, we evaluate whether current data can distinguish between the magnitude distribution of triggered and untriggered small earthquakes. We use a mixing model approach in which total seismicity is decomposed into two classes: "triggered" events initiated or advanced by far-field dynamic strains and "untriggered" spontaneous events consisting of everything else. The *b*-value of a mixed data set, b_{MIX}, is decomposed into a weighted sum of *b*-values of its constituent components, b_T and b_U. We utilize the previously observed relationship between triggering rate and dynamic strain amplitude to identify the fraction of triggered events in populations of earthquakes and then invert for b_T. For Californian seismicity, data are consistent with a single-parameter Gutenberg-Richter hypothesis governing the magnitudes of both triggered and untriggered earthquakes.

1. Introduction

Transient strains delivered by large amplitude seismic waves are frequently associated with seismicity rate increases in the far field at both active margins and stable plate interiors [Hill *et al*., 1993; Velasco *et al*., 2008]. This triggering phenomenon is frequently attributed to dynamic stresses since static stresses decay quickly at such large distances ($\geq$2–3 fault lengths) [King *et al*., 1994]. One of several outstanding problems associated with remote dynamic triggering is whether the magnitudes of triggered earthquakes are significantly different from the magnitudes of ambient seismicity. For instance, *Parsons and Velasco* [2011] investigated whether large ($M \geq 7$) events are capable of dynamically triggering other large ($5 \leq M \leq 7$) earthquakes in the far field and found that they were unable to observe near-instantaneous triggering of large events in the far field. From these observations, they concluded that dynamic stresses must be incapable of affecting faults above a certain length scale. This conclusion was somewhat upended by the 2012 Sumatra-East Indian Ocean earthquake, which triggered over a dozen remote earthquakes of magnitude 5.5–7.0 over the next several days [*Pollitz et al*., 2012]. The question remains as to whether this new observation of large triggered earthquakes reflects an extraordinarily rare event or whether triggered earthquakes simply follow the same size distribution as the population of earthquakes as a whole. In the latter case, the observation of large triggered earthquakes is rare, but expected.

Some of the difficulties in interpreting these intriguing events stem from the relative paucity of large earthquakes in general in the catalog. Since earthquake magnitude distributions generally follow a power law, small earthquakes are much more abundant and amenable to statistical studies than large ones. The magnitude distributions of small earthquakes are also in themselves important for seismicity modeling. Cascade models of earthquake sequences take a parsimonious approach of assuming that triggered earthquakes follow an identical magnitude distribution as untriggered ones [e.g., *Ogata*, 1998]. As a result, the models predict that a cascade of events drawn from a single magnitude distribution can culminate in large, societally significant earthquakes [*Ogata*, 1998; Felzer *et al*., 2002, 2004; *Helmstetter et al*., 2005].

The assumption that the earthquake magnitude distribution is unaffected by the triggering process bears inspection. Assessing the assumption is observationally intricate as it relies on distinguishing the triggered and untriggered populations. Near-field aftershocks from large earthquakes are routinely observed to follow

the standard magnitude distribution, however, the potential for multiple triggering processes and the discovery of remote dynamic triggering has reopened the conundrum as discussed above.

Here we use a new strategy based on estimating the fraction of earthquakes that are triggered following a given dynamic strain. We seek to determine if populations of earthquakes that include many remotely triggered events have a different distribution than those that contain very few triggered earthquakes. We focus our work in this paper on the most common magnitudes of earthquakes, i.e., small events. After an overview of earthquake frequency-magnitude distributions, we will discuss a mixing model that relates the observable *b*-value of a mixed group of triggered and untriggered earthquakes, b_{MIX}, to the parameter of interest (the *b*-value of the triggered events, b_T). Utilizing this model requires constructing populations of earthquakes with an inferred fraction of triggered events. We proceed to form groups of earthquakes that have been affected by dynamic strains of similar amplitude. We then estimate the fraction of triggered events in each of these groups based on the applied strain and invert for b_T.

2. Earthquake Magnitude Distributions

The magnitude-frequency distribution of earthquakes over broad swaths of regions and time can be represented by the cumulative Gutenberg-Richter (GR) distribution

$$\log_{10}(N(m)) = a - b \cdot m \tag{1}$$

where a and b are constants, $N(m)$ is the number of earthquakes with magnitude greater than m, and $m \geq M_C$, with M_C the magnitude of completeness of the catalog [*Ishimoto and Iida*, 1939; Gutenberg and Richter, 1944]. The Aki-Utsu maximum likelihood estimator for the parameter b is

$$b = \frac{\log_{10}(e)}{\langle M \rangle - M_C} \tag{2}$$

where $\langle M \rangle$ is the observed mean magnitude [*Aki*, 1965; Utsu, 1965]. This formulation is appropriate for magnitudes within the power law range of the distribution which is applicable for the small earthquakes considered here.

The Gutenberg-Richter distribution is a representation of the exceedance probabilities for a given range of magnitudes. Characterizing and identifying differences in b-values has implications for both hazard analysis and the physical mechanisms of earthquake nucleation [*Frohlich and Davis*, 1993; Utsu, 1999; *Schorlemmer et al*., 2005]. For constant *a*-value, differences in *b*-value map into differences in the relative hazard of large earthquakes as a function of either space or time for magnitudes up to the maximum magnitude of the underlying distribution. Other parameterizations of the frequency-magnitude distribution are possible, including a truncated distribution that includes maximum magnitude as a free parameter [*Holschneider et al*., 2011]. However, resolving a multivariate distribution requires even more data than resolving differences in *b*-value. As will be shown below, resolving even mean magnitude differences is at the limit of the current data resolution and so no more complex model is warranted by the data.

3. Mixing Model

Suppose a sequence of earthquake magnitudes, M_i^{mix}, exists such that it is composed entirely of either triggered, M_j^T, or untriggered, M_k^U, events. The sum of magnitudes of the mixed (composite) catalog is

$$\sum_{i}^{n_{tot}} M_i^{mix} = \sum_{j}^{n_T} M_j^T + \sum_{k}^{n_U} M_k^U \tag{3}$$

where n_T and n_U are the total number of triggered and untriggered observations, respectively, and $n_{tot} = n_T + n_U$. By dividing both sides by n_{tot} and defining the triggering fraction $f_T \equiv n_T/n_{tot}$, equation (3) can be recast as a weighted sum of the means of the individual components

$$\langle M_{mix} \rangle = f_T \cdot \langle M_T \rangle + (1 - f_T) \cdot \langle M_U \rangle \tag{4}$$

We use equation (2) to substitute into equation (4) to find the equivalent relationship between the *b*-values

$$\frac{1}{b_{MIX}} = f_T \cdot \frac{1}{b_T} + (1 - f_T) \cdot \frac{1}{b_U} \tag{5}$$

where b_T, b_U, and b_{MIX} are the b-values of the triggered, untriggered, and mixed populations, respectively. We then isolate b_T and find

$$b_T = \frac{f_T \cdot b_U}{\frac{b_U}{b_{MIX}} + f_T - 1} \tag{6}$$

Equation (6) is pragmatically useful because the variables on the right-hand side can all be independently estimated. The same result can also be derived using the maximum likelihood method presented in *Kijko and Smit* [2012; Appendix A]. In practice, the form of equation (6) necessitates two regularity conditions to stabilize the inversion and to produce physically meaningful results: the denominator in equation (6) must be greater than 0 and f_T must be greater than 0. For f_T greater than 0, the denominator is greater than 0 if $b_U/b_{MIX} > 1 - f_T$.

To use equation (6), we need to construct populations of earthquakes with differing fractions triggered and then perform two distinct tasks: (1) measure b_{MIX} in the combined population and (2) determine the fraction of triggered events. Additionally, we need to find a group of earthquakes with a very low fraction of triggering in order to estimate the untriggered b-value b_U.

We will accomplish all of these goals by capitalizing on the previous observation that the fraction of triggered events in the far field is a well-defined function of the peak amplitude of the seismic waves, i.e., larger amplitude waves trigger more events [van *der Elst and Brodsky*, 2010]. Therefore, we can construct groups of earthquakes that immediately follow dynamic strains from distant earthquakes. The groups of earthquakes following large amplitude shaking will have a large (and measurable) triggered fraction, f_T, and can be used in conjunction with equation (6) to measure the b-value of triggered earthquakes, b_T. Those following small or extremely distant earthquakes will have a very low triggered fraction and can be used to approximate b_U. Note that this definition of the untriggered population may include many earthquakes that are triggered by other, unidentified local main shocks. It has been proposed elsewhere that the fraction of locally triggered events catalog-wide is large and so essentially any group of earthquakes will contain aftershocks [e.g., Marsan and Lengliné, 2008]. However, for the purpose of this study, we are asking if a group of identifiable, remotely triggered events has magnitude behavior that is distinct from other groups of earthquakes. This is a key question for both operational forecasting and physical understanding of the dynamic triggering process.

4. Data and Analysis Method

We focus our study on California for the period 1 January 2009 to 1 January 2014. The locale was chosen because previous work has already established a useable relationship between dynamic strain amplitudes and rate changes in the region. The time period was chosen because of a California-wide change in the definition of M_L, implemented in 2008 for hypocenters cataloged by the Southern California Seismic Network (SCSN, network code CI) and in January 2009 for seismicity within the Northern California Seismic Network (NCSN, network code NC) [*Hutton et al*., 2010; *Tormann et al*., 2010; *Uhrhammer et al*., 2011]. Data with network codes NC and CI were accessed from the Advanced National Seismic System (ANSS) Catalog (last accessed July 2014, http://www.ncedc.org/). We used the earthquakes in the box defined by 32°N–42°N, 124°W–114°W with depth less than 15 km. *Uhrhammer et al*. [1996, Table 6] previously established an average difference of 0.4 magnitude units between the magnitudes of identical events reported by the Nevada and Northern California networks. Therefore, we restricted our data to only magnitudes reported by the Northern and Southern California networks to ensure consistency. We fit the minimum magnitude of the power law regime of the frequency-magnitude distribution to find the magnitude of completeness which is 1.8 [*Wiemer and Wyss*, 2000]. The calculated completeness is applicable over the high seismicity regions where measurements are dense (compare Figure 1 and supporting information Figure 1). The b-value and 95% confidence level, generated via 5000 bootstrap resamplings, for the combined CI and NC seismicity is 0.87 ± 0.01. As previously documented by *Tormann et al*. [2010], the magnitude recalibration in 2009 makes this b-value less than the commonly quoted value of 1.

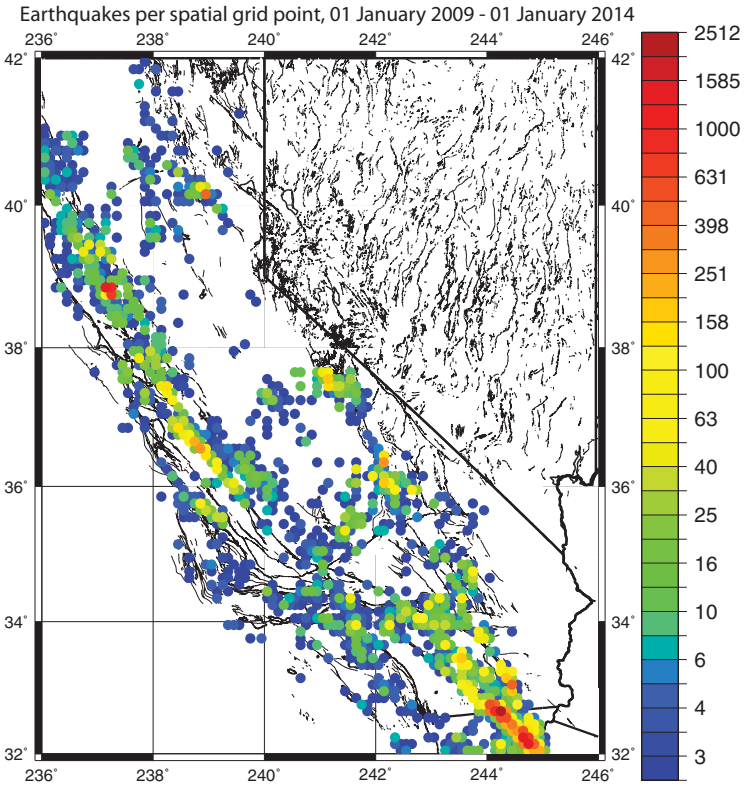

Figure 1. Map of the spatial grid squares with earthquakes of magnitude greater than magnitude 1.8 from 1 January 2009 to 1 January 2014. Colors show number of earthquakes detected at each node. Background image shows state borders and major faults.

In order to identify earthquake populations with strong triggering, we need to estimate the local peak ground velocity from a distant earthquake. We make this estimate by inverting a surface wave magnitude regression appropriate at both regional and teleseismic distances. Our target catalog is partitioned into a $0.1^\circ \times 0.1^\circ$ grid and the effect of each possible trigger is considered on the group of earthquakes in each grid square. For each node, we loop through a global catalog of test triggers. Events with magnitude $M_W > 5$ from the ANSS catalog qualify for inclusion as a test trigger. Depths are limited to those shallower than 100 km because of their greater relative efficiency at generating surface waves. Additionally, each global test trigger must be at least 200 km from a local node.

The previous work of *van der Elst and Brodsky* [2010] used the standard *Ms* attenuation relationship to estimate ground motion for teleseismic earthquakes more than 800 km away based on distance and magnitude. In this study, we use earthquakes as close as 200 km away in order to assemble a sufficiently large set of potential triggers during the period of consistent magnitude determination. Therefore, we require a different attenuation relationship that is more appropriate to the regional distances and is calibrated to be consistent with the teleseismic data. The attenuation relationship of *Russell* [2006] satisfies these criteria and is

$$M_S = \log_{10}(A_\mu) + \frac{1}{2} \cdot \log_{10}(\sin(\Delta)) + 0.0031 \cdot \Delta - \log_{10}(f_c) + 2.57 \quad (7)$$

where A_μ is the zero-to-peak, narrow-band-passed amplitude in microns around the reference period of 20 s, Δ is the epicentral distance in degrees [*Russell*, 2006]. (Note that we convert to microns in equation (7) from the original reference in nanometers.) The parameter f_c corrects for the zero-phase third-order Butterworth filter applied to the data and is equal to $0.03 \cdot (\Delta^{-1/2})$. The drawback of using equation (7) is that the band-pass results in new strain estimates that need to be check for consistency with previous studies. The advantages of having a consistent measure throughout the distance range of interest outweigh this disadvantage for the current use. Since equation (7) is an empirically derived regression, we do not directly use or filter any seismic waveforms; we simply replace the M_S value in the equation with the preferred magnitude for the test trigger as reported by ANSS.

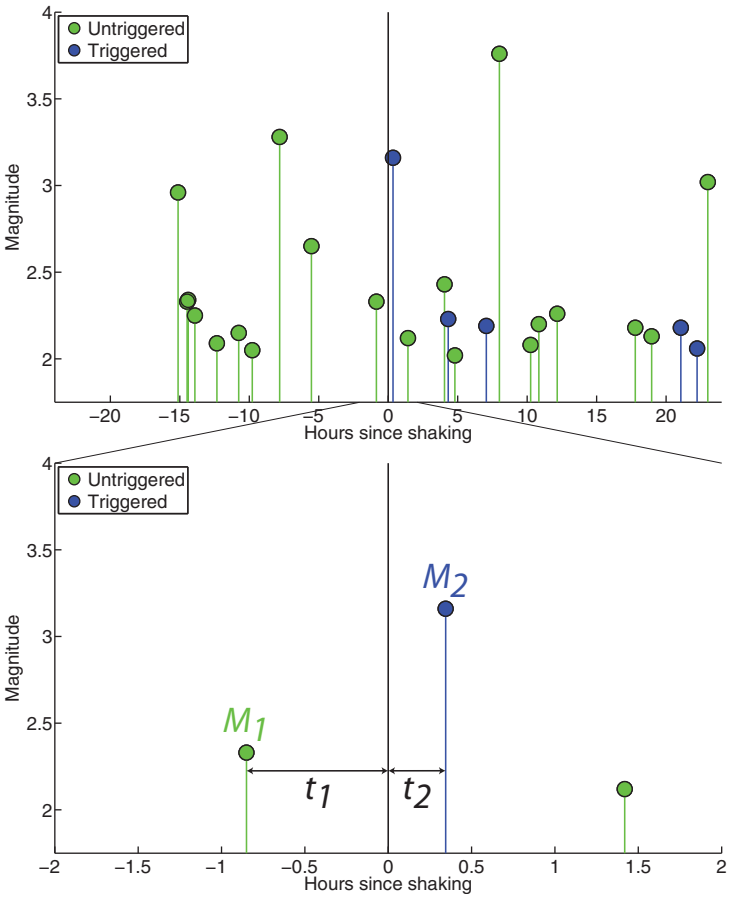

Figure 2. Schematic cartoon of hypothetical synthetic data from a single grid node, demonstrating the procedure for measuring *R*-values. The vertical black line is the approximate arrival time of seismic energy from one far-field event, i.e., "test trigger."

Finally, we estimate strain, ε, by assuming

$$\varepsilon = \frac{V}{C_S} \tag{8}$$

where V is the particle velocity (approximately equal to $2\pi fA$ [*Aki and Richards*, 2002], with A inverted from equation (7)) and C_S is the surface wave group velocity (3.5×10^9 μm/s for Rayleigh waves). Second-order effects due to depth, rupture directivity, and radiation pattern are not captured by these regressions and can result in errors as high as 1 order of magnitude in extreme cases. The global average curve will accurately predict the average strain of a large group of potential triggering events [*Gomberg and Agnew*, 1996].

Once the shaking is known, we can use the previous calibration of fractional seismicity rate changes in California as a function of applied dynamic strain [*van der Elst and Brodsky*, 2010; *van der Elst et al.*, 2013]. For a given source volume with a distribution of faults, *van der Elst and Brodsky* [2010] model the seismicity of the volume as a Poisson process with an average intensity parameter λ. Dynamic strains traveling through a source volume can activate faults and induce a step change in the intensity parameter from λ_1 to λ_2. For a stepwise homogenous Poisson process, the fractional rate change induced by some far-field trigger is

$$\delta\lambda = \frac{\lambda_2 - \lambda_1}{\lambda_1} \tag{9}$$

For a group of target areas that have experienced given amplitudes of shaking, *van der Elst and Brodsky* [2010] and *van der Elst et al.* [2013] showed that

$$\delta\lambda = 82\varepsilon^{0.43} \tag{10}$$

This measurement is based on using the interevent time ratio called the *R*-statistic to measure rate changes [*Felzer and Brodsky*, 2005]. We review the method here as the *R*-statistic is key to our identification of triggered and untriggered earthquake magnitude distributions.

The interevent time ratio is defined as

$$R \equiv \frac{t_2}{t_1 + t_2} \tag{11}$$

where t_1 and t_2 are times to the first earthquakes before (with magnitude M_1) and after (with magnitude M_2) the arrival of seismic energy from some potential far-field trigger (Figure 2). In the absence of triggering, the population of *R*-values will be distributed according to the standard uniform distribution with $\mu = 0.5$ and $\sigma^2 = 1/12$. In the presence of triggering, there will be a bias toward small values of t_2, leading to a larger

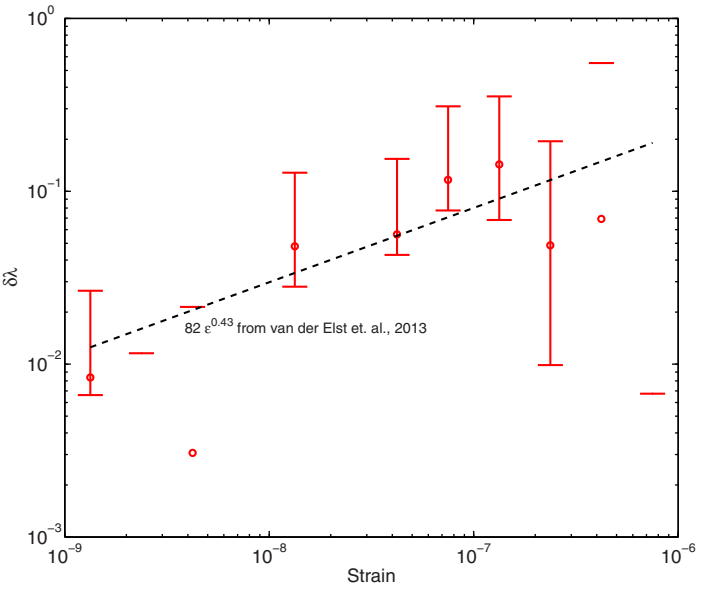

Figure 3. Triggering intensity (fractional rate change, $\delta\lambda$) for the ANSS California seismicity (network codes CI & NC) between 1 January 2009 and 1 January 2014, depths <15 km and a magnitude of completeness 1.8 (red). For each amplitude bin, the finite-catalog-corrected mean *R* ratio was converted to a fractional rate change via equation (12). Error bars are 90% confidence intervals from 1000 bootstrap resamplings of the *R*-values in the amplitude bin.

proportion of small *R*-values and therefore a deflection of the mean value of R, $\bar{R}$, to less than 0.5. In particular,

$$\bar{R}=\frac{1}{\delta\lambda^2}\cdot[(\delta\lambda+1)\cdot\ln(\delta\lambda+1)-\delta\lambda] \tag{12}$$

For any real catalog of earthquakes, the finite observation period introduces a bias in the calculation of *R*-values. Neither t_1 nor t_2 can take on infinite values. The limits on t_1 and t_2 are set by the time of triggering earthquakes. Therefore, *van der Elst and Brodsky* [2010] estimate this bias by generating simulated catalogs at all grid points with uniformly distributed local earthquake times and fixed global trigger times. In each amplitude bin, the deviation of the mean values of *R* in the simulations from 0.5 is subtracted from the mean values of *R* measured prior to applying equation (12) to determine the fractional rate change.

Figure 3 compares the rate changes inferred from the 2009–2014 Californian data set as defined above with the prediction of equation (10). We use 100 local simulations here for the bias-correction and 1000 bootstraps of the *R*-value in each amplitude bin to establish the 90% confidence intervals. The consistency of the current results with the previous work allows us to proceed in using equation (10) with the 2009–2014 data to study triggered magnitude distributions.

5. Fractional Rate Change

Inverting for b_T from the mixing model in equation (6) requires an estimate of the fraction of the data attributed to triggered earthquakes, or f_T. Over one pretrigger recurrence interval (time $\tau=\lambda_1^{-1}$), the number expected in the recurrence interval prior to the test trigger is $n_{before}=\lambda_1\cdot\lambda_1^{-1}=1$. Since we are interested in the amount and type of seismicity in the aftermath of a potential rate change, this can be expressed as

$$n_{after}=\lambda_2\cdot\tau=n_{tot} \tag{13}$$

where again $\tau=\lambda_1^{-1}$ is the relevant time scale we are interested in and n_{tot} is the total number of earthquakes in the interval after the trigger including both triggered and untriggered events. It follows that $n_{tot}=n_{after}=\delta\lambda+1$. With these two definitions of n_{before} and n_{after}, we can therefore define f_T as

$$f_T=\frac{n_T}{n_{tot}}=\frac{n_{tot}-n_U}{n_{tot}}=\frac{n_{after}-n_{before}}{n_{after}}=\frac{(\delta\lambda+1)-1}{\delta\lambda+1}+\frac{\delta\lambda}{\delta\lambda+1} \tag{14}$$

Equation (10) is used to estimate $\delta\lambda$ and therefore f_T with equation (14). Once f_T has been estimated, we then measure the composite *b*-value (b_{MIX}) and proceed to infer a range of values for b_T that is consistent with the data.

6. Sampling Biases

One of the advantages of the *R*-statistic approach to identifying triggered magnitude distribution is the measurements require only that there be uniform detection capability for each local measurement over the

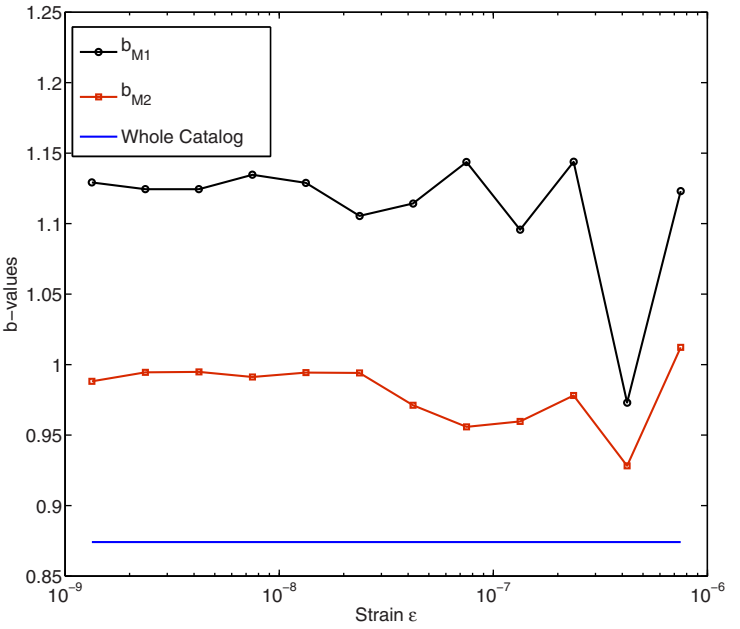

Figure 4. *b*-Values for the M_1 and M_2 populations of data as a function of peak dynamic strain. Both curves show *b*-values higher than the catalog-wide value (solid blue line). The persistent static offset between the three curves is due to the aftershock shielding effect and foreshock shielding effect (see text and Figure 5).

study period. Spatial variability of completeness between grid squares can be tolerated. However, there are other, insidious biases that result because of the conditioning introduced by the *R*-statistic. Here we describe and analyze the effects of these biases which we term aftershock and foreshock shielding.

6.1. Aftershock Shielding Effect

The final requirement to infer b_T is a measurement of b_U, the reference background seismicity parameter. We initially attempted to define b_U using events from the population of M_1 events. In that case, we supposed that the magnitude of the event immediately preceding the arrival of dynamic stress was an accurate representation of the steady state distribution of magnitudes in a system unperturbed by far-field transient waves. However, we found that over the entire range of strain, the bias-corrected M_1 population shows a consistently higher *b*-value (corresponding to a lower mean magnitude) than its equivalent population of bias-corrected M_2 magnitudes (Figure 4). This effect stems from the clustering of earthquakes into aftershock sequences. We therefore call this the aftershock shielding effect. Figure 5 shows a schematic diagram demonstrating the origin of the systematic offset of magnitudes between the measurements of M_1 and M_2. When a larger-than-average earthquake occurs, it tends to generate aftershocks. The time to the first earthquake in this aftershock sequence tends to be shorter than the time to the

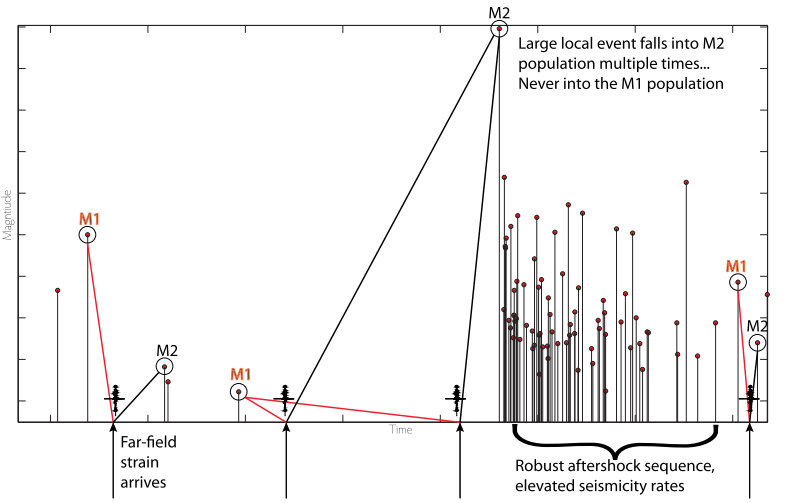

Figure 5. Schematic diagram for the origin of the systematic offset of magnitudes between the M_1s and M_2s. Teleseismic waves arriving in our target catalog are represented by black arrows. For each far-field event, a unique R-ratio is calculated and an M_1 and M_2 within the local catalog are identified. When a local main shock occurs, the time to the next event is, on average, substantially reduced as aftershocks tend to cluster in time and space. It is therefore unlikely that teleseismic surface waves will arrive in the time interval between the local main shock and its first local aftershock. Therefore, the large local main shocks in a target catalog are rarely designated M_1, and almost always designated M_2. Hence, the systematic offset in magnitudes between the two data sets. We call this the aftershock shielding effect.

first earthquake that preceded the main shock. Seismic waves from a distant earthquake are thus much less likely to fall within the latter interval than the former. This means that a large magnitude local main shock is systematically biased to be labeled an "M_2" versus an "M_1." The large main shock is shielded from being labeled an M_1 by its ensuing aftershocks.

6.2. Foreshock Shielding Effect

The presence of foreshocks induces a similar shielding effect. In figure, the *b*-values of the M_2 data are systematically larger than the *b*-value of the overall catalog (∼0.87). Since foreshock sequences follow an Inverse Omori Law, as far-field triggers approach the time of a local main shock, they may fall within the rate increases (in an average sense) that precede the local main shock.

6.3. ETAS Simulation

We can reproduce both of these shielding effects in an epidemic-type aftershock (ETAS) model [*Ogata*, 1998]. Following the procedure of *Brodsky* [2011], we produced a synthetic catalog with a *b*-value of 1 and measured the magnitude distribution of the events prior and after randomly selected times. We found for 100 simulations that the M_1 *b*-value = 1.22 ± 0.04 and the M_2 *b*-value = 1.0 ± 0.03, with 1 standard deviation reported.

As discussed in *Brodsky* [2011], standard ETAS simulations have too few foreshocks (relative to aftershocks) compared to the observations. This disparity is due to either completeness problems or a physical propensity for foreshocks. The overabundance of foreshocks is an interesting issue in itself; however, here we are only concerned with its effect on the sampling of magnitudes. Therefore, since the standard ETAS simulation using standard parameters only reproduced the aftershock shielding and did not explain the deviation of the M_1s in the observations, we performed an additional set of modified ETAS simulations that mimic the large fraction of foreshocks. To illustrate the foreshock abundance of real catalogs, a fraction of the aftershocks were randomly assigned to occur as foreshocks, i.e., the sign of the time from the main shock is reversed. We emphasize that this adaptation of the ETAS model is employed simply as a tool to investigate the effects of foreshocks on selection of earthquakes. If 25% of the aftershocks are turned into foreshocks, the observed aftershock to foreshock ratio was close to the catalog values (∼2) and the observed M_1 *b*-value = 1.19 ± 0.03 (1 std.) and the M_2 *b*-value = 1.10 ± 0.04 (1 std.), which offset approximately 0.1 and 0.2 units from the catalog-wide *b*-value. These offsets from the catalog-wide value are similar to the offsets observed in actual data (Figure 4). We conclude from this exercise that the offsets between the M_1 and M_2 populations can be explained as a natural consequence of the effect of earthquake foreshock and aftershock sequences on selecting earthquakes. No more elaborate hypothesis about triggered magnitudes is necessary.

7. Results

Because of the aftershock and foreshock shielding, we cannot directly compare the M_1 and M_2 magnitudes as a measure of the effect of triggering. Instead, we must define a reference, untriggered mean magnitude from the M_2 data set for comparison to the triggered M_2 magnitudes. We therefore take the values of M_2 corresponding to the lowest fractional rate changes (i.e., $\varepsilon \sim 10^{-9}$) to represent the parameter b_U, equal to 0.99 (Figure 4). Next we apply the mixing model to b_{MIX} data to extract b_T from the three observable variables: b_{MIX}, b_U, and f_T. Figure 6 shows the results of the b_T inversion for the combined catalog. We generate 1000 bootstrap resamplings (sampling with replacement) of the M_2 values in each amplitude bin and use the 50% and 90% confidence intervals on M_2 to derive the confidence intervals shown in Figure 6 [*Efron and Tibshirani*, 1994]. These observations suggest that *b*-values of data with high percentage of triggered earthquakes have no obvious trend relative to the *b*-values of untriggered or spontaneous seismicity. The differences with the overall *b*-value of the data set are insignificant and cannot be distinguished from background seismicity.

It is tempting to further disaggregate the data and exam whether or not particular regions might have a magnitude distribution change. However, the ability to distinguish b_T from b_U relies on the ability to measure the triggered fraction f_T. As shown by *van der Elst et al*. [2013], there is a strong trade-off between the number of measurements and the resolution of rate changes and so we are limited to the aggregate data set that provides sufficient population sizes for robust measurements.

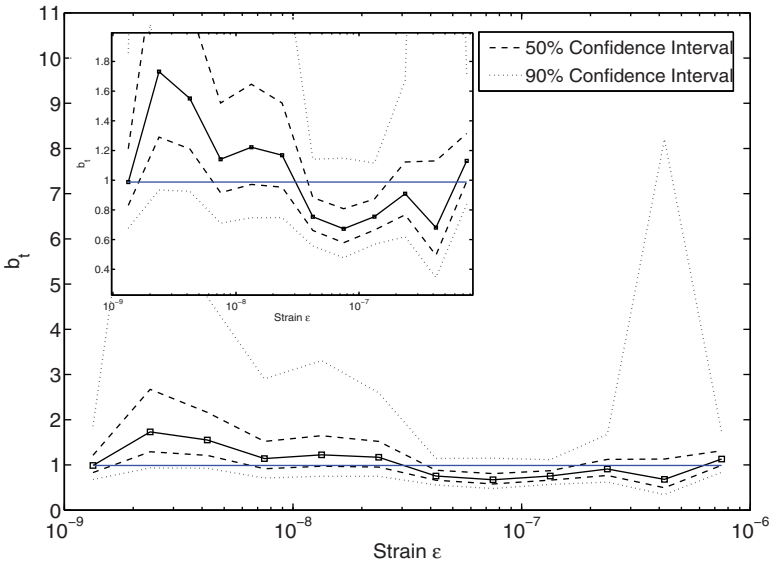

Figure 6. b_T as inverted from equation (6), with inset showing an expanded version. The horizontal line corresponds to an estimate of b_U based on data from the strain measurements in the smallest amplitude bin. Error bars derived from 5000 bootstraps indicate the triggered *b*-values (b_T) are insignificantly different from our reference b_U.

8. Implications

Our results indicate there are no discernible differences between the magnitude distributions of data sets that likely contain a high proportion of triggered events, versus data sets that do not contain high proportions of triggered events. The observed composite *b*-values (b_{MIX}, red curve in Figure 4) show no significant variation with respect to calculated peak dynamic strains (Figure 4). The small variations that do exist do not show a monotonic trend with the fraction of likely triggered events in the population, meaning that this conclusion is not likely to change with increased statistical resolution. Inverting for b_T directly using a mixing model does not alter these conclusions (Figure 6).

These interpretations are significantly different than that of *Parsons and Velasco* [2011] who suggested that dynamically triggered earthquakes are preferentially small. These studies differ in fundamental ways. For instance, the statistical treatment here includes greater than 400 examples of potential triggers for each data set, including some very weak triggers, and deals explicitly with the fact that any observed group of earthquakes is a mixture of triggered and untriggered events via our mixing model. The previous work had 205 examples of very strong triggering. Second, the R-statistic uses an optimized, adaptive time window to measure rate changes and therefore is inherently more sensitive than the counting method of Parsons and Velasco. Finally (and perhaps most importantly), we focus on small earthquakes as diagnostic of the magnitude distribution; this contrasts with the approach of Parsons and Velasco where only $5 < M_W < 7$ events are examined. The advantage of this paper's approach is that larger numbers ensure statistical robustness since larger magnitude earthquakes are intrinsically rare and may not be observed during a short time interval.

The current results more directly constrain the cascade behavior of earthquake sequences. The current data suggest that a single magnitude distribution is adequate to capture the triggering behavior from dynamic waves and therefore an ETAS-style model is an appropriate tool to evaluate the expected consequence of shaking.

9. Conclusions

We find that no statistical evidence for fundamentally different underlying distributions between triggered and untriggered earthquakes. This supports the idea that the magnitudes of triggered and untriggered earthquakes are randomly drawn from a single-parameter GR distribution over the studied magnitude range. Remotely triggered earthquakes are likely to be as large as any other group of seismicity. However, since the total number of triggered events is small, the probability of observing a remotely triggered large

earthquake is accordingly small. Cascade models drawn from a single magnitude distribution are consistent with the dynamically triggering data as currently available.

Acknowledgments
Waveform data, metadata, or data products for this study were accessed through the Northern California Earthquake Data Center (NCEDC). This work was funded in part by an NSF Graduate Fellowship DGE-0809125 to S. Hernandez and NSF Award EAR-0838598 to Brodsky.

References

Aki, K. (1965), Maximum likelihood estimate of b in the formula log N = a − bM and its confidence limits, *Bull. Earthquake Res. Inst. Tokyo Univ.*, *43*, 237–239.
Aki, K., and P. G. Richards (2002), *Quantitative Seismology*, 2nd ed., 700 pp., Univ. Sci. Books, Sausalito, Calif.
Brodsky, E. E. (2011), The spatial density of foreshocks, *Geophys. Res. Lett.*, *38*, L10305, doi:10.1029/2011GL047253.
Efron, B., and R. J. Tibshirani (1994), *An Introduction to the Bootstrap, Monogr. Stat. Appl. Probab.*, 436 pp., CRC Press, Boca Raton, Fla.
Felzer, K. R., and E. E. Brodsky (2005), Testing the stress shadow hypothesis, *J. Geophys. Res.*, *110*, B05S09, doi:10.1029/2004JB003277.
Felzer, K. R., T. W. Becker, R. E. Abercrombie, G. Ekstrom, and J. R. Rice (2002), Triggering of the 1999 MW 7.1 Hector Mine earthquake by aftershocks of the 1992 MW 7.3 Landers earthquake, *J. Geophys. Res.*, *107*(B9), 2190, doi:10.1029/2001JB000911.
Felzer, K. R., R. E. Abercrombie, and G. Ekstrom (2004), A common origin for aftershocks, foreshocks, and multiplets, *Bull. Seismol. Soc. Am.*, *94*, 88–98.
Frohlich, C., and S. D. Davis (1993), Teleseismic *b* values; or much ado about 1.0, *J. Geophys. Res.*, *98*(B1), 631–644, doi:10.1029/92JB01891.
Gomberg, J., and D. Agnew (1996), The accuracy of seismic estimates of dynamic strains: An evaluation using strainmeter and seismometer data from Pinon Flat Observatory, California, *Bull. Seismol. Soc. Am.*, *86*, 212–220.
Gutenberg, B., and C. F. Richter (1944), Frequency of earthquakes in California, *Bull. Seismol. Soc. Am.*, *34*(4), 185–188.
Helmstetter, A., Y. Y. Kagan, and D. D. Jackson (2005), Importance of small earthquakes for stress transfers and earthquake triggering. *J. Geophys. Res.*, *110*, B05S08, doi:10.1029/2004JB003286.
Hill, D. P., et al. (1993), Seismicity remotely triggered by the magnitude 7.3 Landers, California, earthquake, *Science*, *260*(5114), 1617–1623.
Holschneider, M., G. Zoller, and S. Hainzl (2011) Estimation of the maximum possible magnitude in the framework of a doubly-truncated Gutenberg-Richter model, *Bull. Seismol. Soc. Am.*, *101*, 1649–1659.
Hutton, K., J. Woessner, and E. Hauksson (2010), Earthquake monitoring in Southern California for seventy-seven years (1932–2008), *Bull. Seismol. Soc. Am.*, *100*, 423–446.
Ishimoto, M., and K. Iida (1939), Observations of earthquakes registered with the microseismograph constructed recently, *Bull. Earthquake Res. Inst. Univ. Tokyo*, *17*, 443–478.
Kijko, A., and A. Smit (2012), Extension of the Aki-Utsu b-value estimator for incomplete catalogs, *Bull. Seismol. Soc. Am.*, *102*, 1283–1287.
King, G. C. P., R. S. Stein, and J. Lin (1994), Static stress changes and the triggering of earthquakes, *Bull. Seismol. Soc. Am.*, *84*, 935–953.
Marsan, D., and O. Lengliné (2008), Extending earthquakes' reach through cascading, *Science*, *319*, 1076–1079.
Ogata, Y. (1998), Space-time point-process models for earthquake occurrences, *Ann. Inst. Stat. Math.*, *50*(2), 379–402.
Parsons, T., and A. A. Velasco (2011), Absence of remotely triggered large earthquakes beyond the mainshock region, *Nat. Geosci.*, *4*, 321–316, doi:10.1038/ngeo1110.
Pollitz, F. F., R. S. Stein, and R. Burgmann (2012), The 11 April 2012 M = 8.6 East Indian Ocean earthquake triggered large aftershocks worldwide, *Nature*, *490*, 250–253, doi:10.1038/nature11504.
Russell, D. R. (2006), Development of a time-domain variable-period surface-wave magnitude measurement procedure for application at regional and teleseismic distances, part I: Theory, *Bull. Seismol. Soc. Am.*, *96*, 665–677.
Schorlemmer, D., S. Weimer, and W. Wyss (2005), Variations in earthquake-size distribution across different stress regimes, *Nature*, *437*, 539–542, doi:10.1038/nature04094.
Tormann, T., S. Wiemer, and E. Hauksson (2010), Changing of Reporting Rates in the Southern California Earthquake Catalog, introduced by a New Definition of ML, *Bull. Seismol. Soc. Am.*, *100*, 1733–1742.
Uhrhammer, R. A., S. J. Loper, and B. Romanowicz (1996), Determination of local magnitude using BDSN broadband records, *Bull. Seismol. Soc. Am.*, *86*, 1314–1330.
Uhrhammer, R. A., M. Hellweg, K. Hutton, P. Lombard, A. W. Walters, E. Hauksson, and D. Oppenheimer (2011), California Integrated Seismic Network (CISN) local magnitude determination in California and vicinity, *Bull. Seismol. Soc. Am.*, *101*, 2685–2693.
Utsu, T. (1965), A method for determining the value of b in the formula log n = a − bM showing the magnitude-frequency relation for earthquakes [in Japanese with English summary], *Geophys. Bull. Hokkaido Univ.*, *13*, 99–103.
van der Elst, N. J., and E. E. Brodsky (2010), Connecting near-field and far-field earthquake triggering to dynamic strain, *J. Geophys. Res.*, *115*, B07311, doi:10.1029/2009JB006681.
van der Elst, N. J., E. E. Brodsky, and T. Lay (2013) Precursory remote triggering is absent near the epicenters of great earthquakes, *Bull. Seismol. Soc. Am.*, *103*, 1522–1540, doi:10.1785/0120120126.
Velasco, A. A., S. Hernandez, T. Parsons, and K. Pankow (2008), Global ubiquity of dynamic earthquake triggering, *Nat. Geosci.*, *1*, 375–379.
Wiemer, S., and M. Wyss (2000), Minimum magnitude of completeness in earthquake catalogs: Examples from Alaska, the western United States, and Japan. *Bull. Seismol. Soc. Am.*, *90*(4), 859–869.